Residual stress gradient and relaxation upon fatigue deformation of diamond-like carbon coated aluminum alloy in air and methanol environments

Nedunchezhian Srinivasan [a], Lalith Kumar Bhaskar [a], Ravi Kumar [a,*], Sergio Baragetti [b,c]

[a] Laboratory for High Performance Ceramics, Department of Metallurgical and Materials Engineering, Indian Institute of Technology Madras, Chennai 600036, India
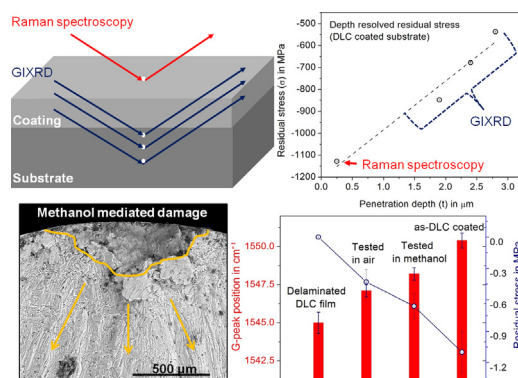[b] Department of Management, Information and Production Engineering, University of Bergamo, Viale Marconi 5, Dalmine 24044, Italy
[c] GITT – Centre on Innovation Management and Technology Transfer, University of Bergamo, Via Salvecchio 19, Bergamo 24129, Italy

HIGHLIGHTS

- Diamond-like amorphous carbon was coated over the aluminum alloy substrate using magnetron sputtering technique.
- Residual stress profile of coated substrates up to 3 μm in depth measured using non-destructive techniques.
- Role of chemical environment revealed through poor fatigue performances of specimens tested in methanol environment.
- Good correlations exist between residual stress relaxation upon fatigue loading and the fatigue properties of the material.

GRAPHICAL ABSTRACT

ARTICLE INFO

ABSTRACT

Amorphous diamond-like carbon coating (DLC) of 2 μm in thickness was deposited over the aluminum alloy substrate using magnetron sputtering deposition technique. In order to understand the efficacy of coating deposition, coated specimens were subjected to rotating bending fatigue in air and methanol environments respectively. Raman spectroscopy was used in conjunction with grazing incidence X-diffraction technique to obtain depth-resolved residual stress gradients of coated-aluminum substrate. The residual stress generated due to coating deposition was calculated using Raman spectroscopy and it was −1.13 ± 0.16 GPa (compressive in nature). Furthermore, Raman spectroscopy was utilized for the quantification of stress relaxation upon fatigue loading in air and methanol environments. It was observed that the irrespective of the testing environment, good correlation exists between the stress relaxation magnitude and number of cycles endured before failure.

1. Introduction

Aluminum alloys are widely used in automotive and aerospace applications mainly due to its high specific strength, in contrast to conventional structural alloys such as steels [1]. However high strength aluminum alloys especially 7000 series alloys in T6 temper condition,

* Corresponding author.
E-mail address: nvrk@iitm.ac.in (R. Kumar).

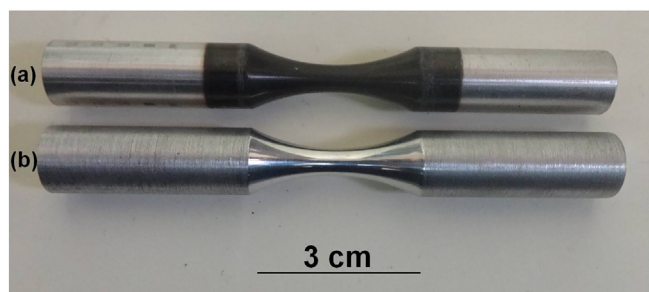**Fig. 1.** Photograph of (a) DLC coated and (b) uncoated fatigue specimens prior to testing.

Table 1
Peak intensity ratios as a function of incidence angle (α).

Grazing incidence angle (α)	Peak intensity ratio (I/I_{max})			
	(111)	(200)	(220)	(311)
5	100	15.5	2.2	5.7
7	100	15.9	1.7	5.2
8.5	100	16.7	1.9	5.6

also suffers from inherent drawback such as poor corrosion resistance. Furthermore, when such alloys were exposed to a combination of corrosive environment and fatigue loading during its service, severe reduction in mechanical properties was reported [1]. Very limited literature reported the influence of combined effect of fatigue loading and corrosive environment on the performance of 7000 series alloys. The source of fracture/fatigue crack initiation was due to formation of corrosion pits on the surface of the alloy, when exposed to aggressive environments. In order to mitigate the influence of environment on the fatigue performance of structural alloys, anodizing or surface coatings techniques were carried out to improve hardness, wear resistance as well as corrosion resistance. However, one of the drawbacks of surface anodization was the generation of cracks and defects during surface pretreatment and etching processes, which will act as preferential sites for crack nucleation. It was already reported that sulfuric acid anodization of 7075-T73 aluminum alloy resulted in 60% percent reduction in fatigue life [2].

Surface coatings are envisaged for the corrosion protection of aluminum substrates such as TiN, ZrN, WC/C, Ni-P and DLC based PVD coatings to improve fatigue performance in corrosive environments [3–7]. TiN/ZrN based hard PVD coating involves coating deposition at a temperature of around T = 400 °C, which is close to solutionizing temperature of the AA-7075-T6 aluminum alloy. Such high deposition temperature was needed to achieve superior hardness and wear resistance [6,7]. However, this also results in loss of mechanical properties of the substrate, due to the dissolution of precipitates, when exposed to such high deposition temperatures. Furthermore, to restore the mechanical properties, post-deposition heat treatment is necessary to

improve tensile and fatigue properties [8]. Thus, low temperature PVD deposition process (without additional post-deposition heat treatment) is beneficial in improving surface properties, without compromising the mechanical properties of the substrate material.

Diamond-like carbon (DLC) coatings are promising in nature, since superior properties are achieved at lower deposition temperatures. Diamond-like carbon is a metastable form of carbon contains significant fraction of sp^3 bonds and possess higher hardness, elastic modulus, chemical inertness and good semiconductor properties [9]. Hence, DLCs are widely used as protective coatings in wide variety of applications such as magnetic storage disks, micro-electronic mechanical devices and biomedical applications. DLCs are amorphous in nature and depending upon the nature of hydrocarbon atmosphere and processing conditions, hydrogen content can be altered to fine-tune the mechanical and band gap properties of the films. Deposition techniques such as magnetron sputtering, ion-beam, cathodic arc technique, plasma enhanced chemical vapor deposition (PECVD) are widely used to coat DLC on various substrates [9]. In addition, deposition parameters can be altered to achieve the desired hardness, Young's modulus and density of the coating by tailoring sp^2/sp^3 ratio, sp^2 clustering and its orientation [10]. Furthermore, transition metals [W, Cr and Ti] can be incorporated in to DLCs to improve adhesion over the metallic substrates [11].

In addition to improved surface properties, compressive residual stresses were generated due to low temperature DLC coating deposition and it may influence the mechanical properties of the coated substrates, especially fatigue properties. Moreover, it was already reported that for amorphous carbon coated austenitic steel substrate, 300% improvement in fatigue life at lower strain amplitudes in contrast to uncoated samples [12]. Hence, it is of paramount importance, to study the nature and magnitude of residual stresses generated due to DLC coating deposition and its influence on mechanical behavior during fatigue loading of aluminum alloys. Since, DLC layer is amorphous in nature; X-ray diffraction technique cannot be used for the measurement of residual stresses of the coating.

Residual stresses in DLCs were often measured from curvature measurements by coating a DLC layer on thin substrates (glass or silicon wafers) and measuring the beam curvature/deflection before and after the
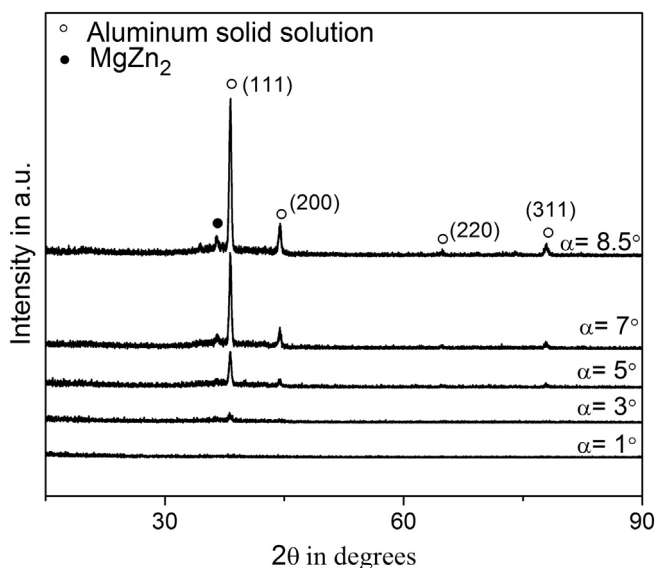

Fig. 2. Grazing incidence XRD of DLC coated aluminum substrate at various incidence angle (α).
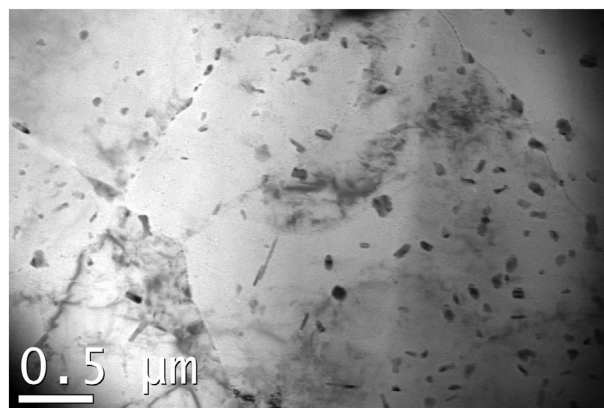

Fig. 3. Representative TEM of extruded and artificially aged aluminum alloy showing precipitate morphology and distribution.
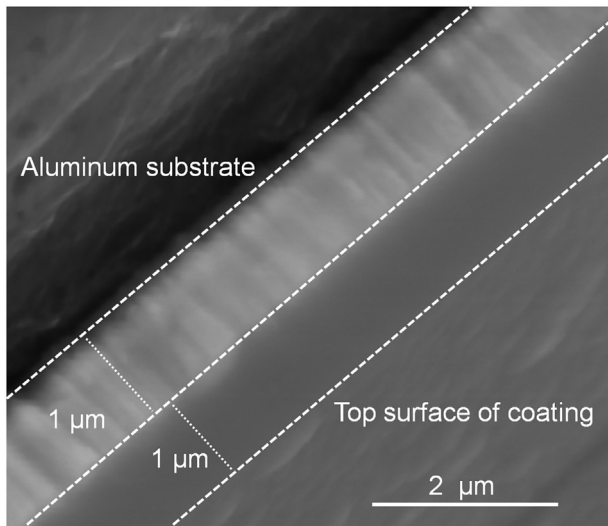
Fig. 4. SEM of DLC coated aluminum substrate revealing 2 micron thick bilayer.

Fig. 5. Nano-indentation curves of DLC coating and the aluminum substrate.

coating deposition [13]. However, these techniques need simple geometries and cannot be extended to fatigue test specimens for correlating residual stresses with the obtained mechanical behavior of the substrate under fatigue conditions. FIB-DIC technique is attractive in measuring in-situ localized residual stresses; however it involves complex testing methodologies and suitable relaxation geometry for the measurement of relief strains [14,15]. Hence, non-destructive Raman spectroscopy [16,17] can be of vital significance to measure and correlate the residual stresses on fatigue properties, without resorting to complex sample fabrication procedures for the measurement of residual stresses.

The present work investigates the fatigue behavior of DLC coated and uncoated 7075 aluminum alloy in T6 temper condition in air and methanol environments. Fatigue testing was carried out in methanol environment, because it was already reported that stress corrosion cracking resulted in reduction in service life of light alloys especially titanium, when exposed to aggressive chemical environment such as methanol [18]. Residual stress gradient generated due to coating deposition were quantified using Raman spectroscopy for DLC coating and X-ray diffraction technique for obtaining substrate residual stresses. Fractographic analyses of tested samples were carried out to understand the influence of environment and substrate surface condition prior to coating on fatigue behavior of aluminum alloy in air and methanol environments.

2. Materials and methods

AA7075-T6 test specimens were DLC coated using reactive magnetron sputtering technique using WC target in a hydrocarbon atmosphere. The photograph of coated and uncoated specimens before being subjected to testing is shown in Fig. 1a and b. The test specimens were subjected to rotating bending fatigue (stress ratio R = 0.1) in ambient air and methanol environments respectively. Step loading technique was used to determine the limiting threshold stress for initiation of fatigue failure in air and corrosive environments. Detailed experimental procedures with respect to testing in methanol environment can be found elsewhere [18]. Aluminum alloy with two different surface conditions, one with polished using 1200 emery (rough surface) and the other with diamond

polished (smooth surface) were chosen to study the influence of surface finish on coating adhesion and fatigue behavior.

Grazing incidence X-ray diffraction (GIXRD) studies were carried out in Rigaku Smartlab diffractometer using Cu K$_\alpha$ radiation. Göbel mirror was used to achieve parallel X-ray beam configuration. The voltage and current settings were 40 kV and 100 mA respectively. Grazing incidence angles (α) varying from 1° to 8.5° was used to probe the residual stresses in DLC coated aluminum substrates. X-ray diffractograms were obtained in the range of 15°–90° (2θ) with a step size of 0.01° and scan speed of 5.5°/min respectively. The inter-planar spacings (d$_{hkl}$) of diffracted aluminum peaks were obtained using X'pert high score software by fitting with Pearson VII function.

Transmission electron microscopy (TEM) was carried out using 120 kV Philips CM 12 electron microscope for studying the size and morphology of the precipitates. Thin disks of 3 mm diameter of as-received extruded and aged samples were prepared and subjected to ion milling (Gatan PIPS equipment operating at 4.5 keV) to achieve electron transparent regions.

Raman analysis of DLC coated samples was carried out using a LabRAM HR800 visible μ-Raman spectrometer (Horiba Jobin-Yvon) equipped with an Olympus BX41 microscope having an objective lens magnification of 50× respectively. The samples were excited with an argon-ion laser of 488 nm wavelength and signals were obtained in the range of 600 cm^{-1} to 2400 cm^{-1} using 5 mW power supply. Calibration was carried out using a standard [100] preferentially orientated silicon wafer and the standard value of 520.7 ± 0.5 cm^{-1} was ensured prior to analysis. A Gaussian-Lorentzian polynomial function was used for fitting the obtained broad asymmetric spectrum of convoluted G and D peaks of DLC carbon, after background correction using LabSpec Raman spectroscopy software.

The indentation hardness (H) and the reduced elastic modulus (E$_r$) of DLC coating and aluminum substrate were determined using an instrumented depth-sensing nanoindenter (Hysitron Inc., USA). Trapezoidal loading sequence (Berkovich indenter) was used with a holding time of about 10 s at the maximum applied load (P$_{max}$) of 4 mN. The load was chosen in such a way that, the penetration depth of indenter did not exceed 100 nm, which is <1/10th of the DLC coating thickness,

Table 2
EDS compositional analysis of DLC coated aluminum substrate in weight percentage.

	C	W	Ti	Cr	Al
First layer (close to substrate)	55.2	31.2	0.75	2.8	10.0
Second layer	81.9	15.6	–	0.5	2.0

Table 3
Nano-indentation properties of DLC coating and aluminum substrate.

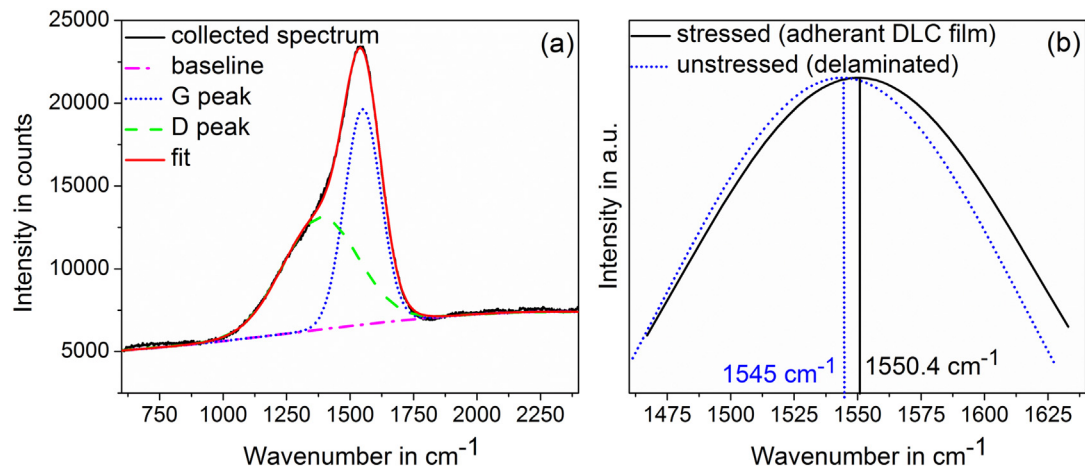| S. no	Property	DLC coating	Aluminum substrate
1.	Hardness in GPa	15.8 ± 1.4	1.95 ± 0.05
2.	Reduced modulus in GPa	162 ± 14	82.6 ± 2.2
3.	Maximum penetration depth in nm	80	252
4.	Contact depth in nm	45	229

Fig. 6. (a) Convoluted Raman peaks of DLC coating (b) Raman peak shift of stressed DLC film.

to avoid the influence of substrate on coating properties. To probe the variation of reduced elastic modulus and hardness as a function of depth from the surface, measurements were taken at the cross-section of coated aluminum samples at regular intervals. The samples were well polished with various grades of emery sheets, followed by diamond polishing (0.25 μm) to achieve smooth surface finish. The Poisson's ratio of the DLC coating was assumed to be 0.3 for the calculation of the elastic modulus of the coating from the obtained reduced modulus (E_r).

The fractography of fatigue fractured samples were carried out using scanning electron microscopy (Quanta 400, USA) in backscattered (BSE) mode using a solid-state detector. Energy dispersive spectroscopy (EDS) using Si(Li) detector was carried out for elemental and compositional analysis of DLC coatings, precipitates and dispersoids.

3. Results

3.1. Characterization of the coating/substrate system

Grazing incidence X-ray diffractograms of DLC coated aluminum substrate at various incidence angles are shown in Fig. 2. At incidence angles 1° and 3°, X-ray amorphous nature of DLC coating is clearly evident. At higher incidence angles ($\alpha \geq 5°$) aluminum substrate peaks were observed in addition to low intense peaks of $MgZn_2$ precipitates.

Furthermore, the intensity ratios (I/I_{max}) of aluminum substrate peaks as a function of grazing incidence angle (α) were calculated [19–22]. No significant changes in I/I_{max} ratio were observed with respect to grazing incidence angle (α) as shown in Table 1. This corroborates the absence of crystallographic transformations in the substrate material during coating deposition.

The ultra-fine grain nature of extruded and aged sample was revealed by TEM with an average grain size of aluminum matrix is about 2 μm (Fig. 3). Furthermore, uniform distribution of $MgZn_2$ precipitates with an average size of about 60 ± 12 nm were observed in the grain interiors as well as along the grain boundaries (Fig. 3). In addition to precipitation strengthening, grain size refinement (Hall-Petch effect) resulted in superior mechanical properties of the substrate material.

Scanning electron micrograph of coating-substrate system (Fig. 4) revealed morphologically distinct bi-layer of 2.0 μm in thickness, coated over the aluminum substrate to achieve good adhesion. Layer close to aluminum substrate is columnar and rich in tungsten, over which
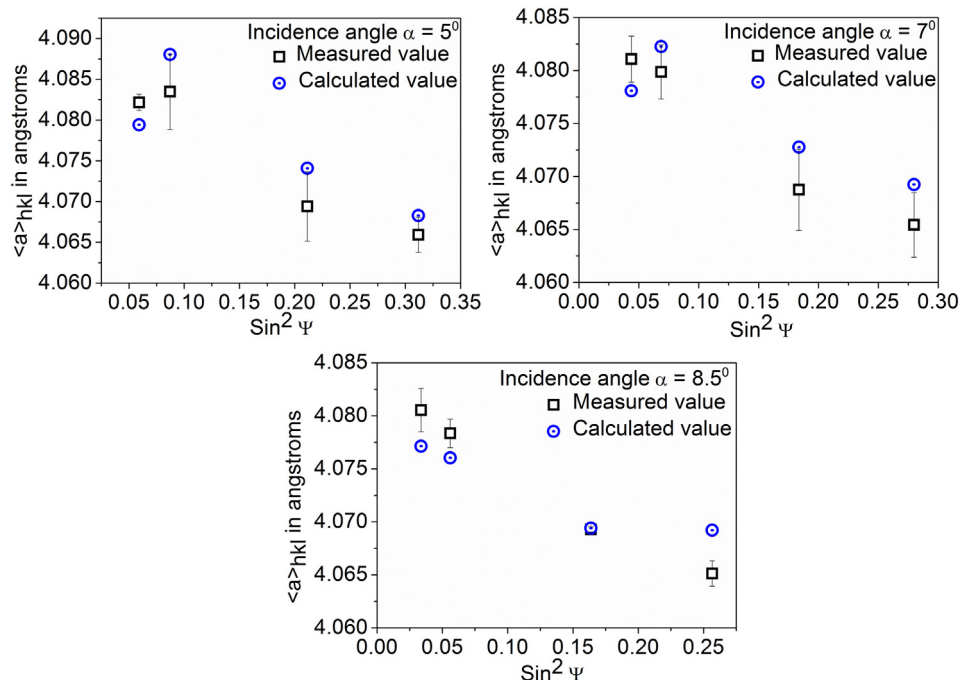

Fig. 7. Comparison of measured and calculated values of lattice parameter $a_{<hkl>}$ at various incidence angles.

carbon-rich DLC layer of 1 micron thickness is coated using magnetron sputtering technique. The composition of tungsten rich layer is 55.2 wt% C, 31.2 wt% W, 0.75 wt% Ti and 2.8 wt% Cr and the composition of the carbon-rich layer is 81.9 wt% C, 15.6% W and 0.5 wt% Cr (Table 2). Tungsten incorporation in to the DLC layer causes the relaxation of distorted C—C bonds, in addition to the formation of weak W—C carbon bonds resulting in significant reduction in residual stresses [23]. Columnar morphology (Zone II of the Thornton's Structure Zone Model) in the tungsten rich layer was attributed to growth phenomenon during the initial stages of sputtering deposition [24]. Small hillocks due to coating deposition were seen on the top surface of the coating. Cr interlayer of nanometer thickness is introduced to improve interfacial strength of W containing amorphous carbon (a-C: H) coating over the metallic substrate.

Nano-indentation responses of DLC coating and the aluminum substrate for the same applied load of 4 mN are shown in Fig. 5 and the obtained nano-indentation properties are displayed in Table 3. It is evident from Fig. 5 that the coating is very hard and stiff and displayed significant elastic recovery in contrast to aluminum substrate.

3.2. Coating residual stress measurement using Raman spectroscopy

Residual stress is quantified by measuring the shift of G peak position of stressed material with respect to the unstressed condition [16,17]. The convoluted D and G peak of DLC coating in stressed condition is shown in Fig. 6a. The obtained spectral shape is a typical example of an hydrogenated a-C:H carbon. The residual stress is calculated from the following formulation:

$$\omega_\tau - \omega_0 = \frac{1}{2\omega_0}(2A\varepsilon_{xx}) = \frac{A}{\omega_0}(S_{11} + S_{12})\sigma \qquad (1)$$

ω_τ is the G-peak position of the stressed material. The value of ω_0 is 1545 cm^{-1} (unstressed) and is obtained by delaminating DLC film (free-standing) from the aluminum substrate through mechanical means. The value of constant A is -1.44×10^7 cm^{-2} and graphite elastic constants $S_{11} = 0.98 \times 10^{-12}$ Pa^{-1} and $S_{12} = -0.16 \times 10^{-12}$ Pa^{-1} are used for the calculations [16].

Irrespective of type of carbon, bonding disorder and excitation wavelength used, G-band is always reflected in Raman spectrum of carbon-based materials and hence G-band peak shift is utilized for residual stress calculation. The G-band is centered on 1545 ± 0.5 cm^{-1} for the stress-free DLC and it was attributed to E_{2g} bond stretching of pair of sp^2 atoms in aromatic and carbon chains. The additional D-
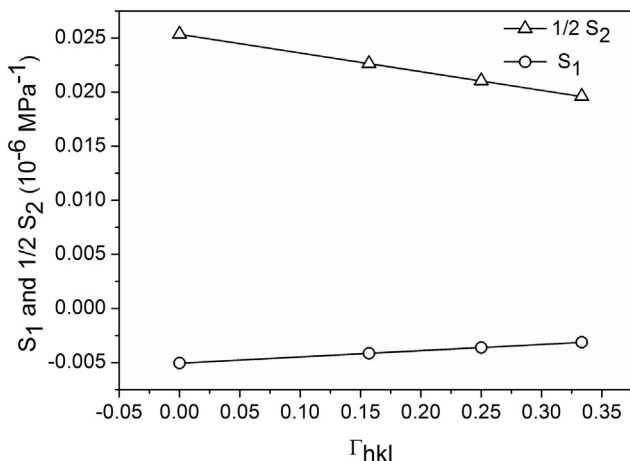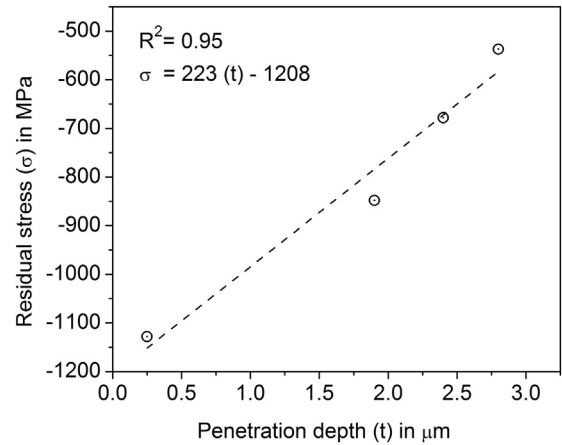

Fig. 9. Residual stress gradient obtained using XRD and Raman as a function of penetration depth.

band is due to disorder in the sp^2 structure and it is attributed to A_{1g} symmetry breathing mode of sp^2 atoms only in the ring structure [25].

Fig. 6b shows the Raman spectroscopy of delaminated DLC film (stress-free) and the film adherent on the substrate (stressed). The shift in peak (towards higher frequency) is clearly observed with respect to the unstressed condition, corroborating the compressive nature of the deposited films. Since, the DLC film is disordered in nature and contains a mixture of sp^2 (graphite-like) and sp^3 (diamond-like) bonds, a stress conversion factor of 4.86 cm^{-1}/GPa was used for the calculation of residual stresses. This is in contrast to the stress conversion factor of 7.7 cm^{-1}/GPa reported for the crystalline graphite [16]. The residual stress calculated using Eq. (1) is -1.13 ± 0.16 GPa (compressive in nature).

3.3. Subsurface substrate residual stress measurements using GIXRD

For the measurement of subsurface substrate residual stresses, multi-reflection grazing incidence technique is used. The method is discussed briefly in this section and a detailed description of the method can be found elsewhere [26]. Using thin-film attachment, measurements were carried out in grazing incidence X-ray diffractometer,
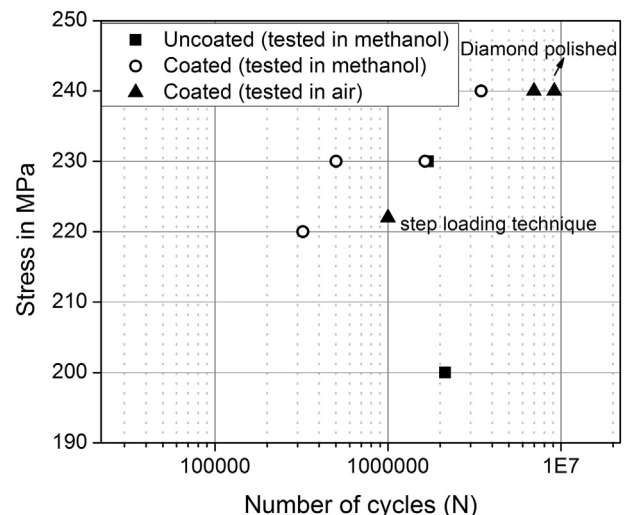

Fig. 8. Diffraction elastic constants as a function of anisotropic parameter $\Gamma_{(hkl)}$.

Fig. 10. Fatigue properties of coated and uncoated AA 7075 alloy in air and methanol [4].
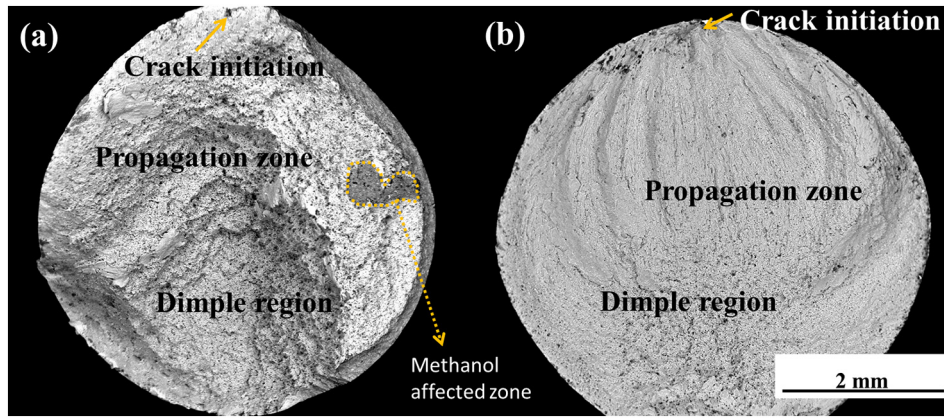
Fig. 11. Overall fracture surface of fatigue failed specimens in methanol (a) uncoated and (b) DLC coated.

after precise Z-alignment of the sample. The residual stress is calculated quantitatively using the equation mentioned below (Eq. (2))

$$<a(\phi,\psi)>_{\{hkl\}} = \left[S_1(hkl)(\sigma_{11}+\sigma_{22}+\sigma_{33}) + \frac{1}{2} S_2(hkl) \right. \quad (2)$$
$$\times \left(\begin{array}{c} \sigma_{11} \cos^2\phi + \sigma_{22}\sin^2\phi \\ + \sigma_{12}\sin2\phi \end{array} \right) \sin^2\psi + \frac{1}{2} S_2(hkl)\sigma_{33}\ \cos^2\psi$$
$$\left. + \frac{1}{2} S_2(hkl)(\sigma_{13}\cos\phi + \sigma_{23}\sin\phi)\ \sin2\ \psi \right] a_o + a_o$$

Assuming a plane stress ($\sigma_{33} = \sigma_{13} = \sigma_{23} = 0$) and an equi-biaxial condition ($\sigma_{11} = \sigma_{22}$) and since all experiments were carried out at $\phi = 0°$ (rotation about z-axis), Eq. (2) is further simplified to

$$<a(\phi,\psi)>_{\{hkl\}} = \left[S_1(hkl)(2\sigma_{11}) + \frac{1}{2} S_2(hkl) \times (\sigma_{11})\ \sin^2\psi \right] a_o$$
$$+ a_o \quad (3)$$

where <a (φ, ψ)>_{\{hkl\}} refers to lattice parameter of a material in stressed state and a_o refers to unstressed lattice parameter of the material. The scattering vector is given by $\psi_{(hkl)} = \theta_{(hkl)} - \alpha$, where, α is the grazing incidence angle. Ψ is defined as the angle between the surface normal and the diffracting plane normal in a ω-goniometer (Eq. (3)). For the given 2θ range (15°–90°) and for a given incidence angle α, the scattering vector $\psi_{(hkl)}$ depends on the (hkl) plane of aluminum substrate, which satisfies the Bragg condition. In the case of aluminum, the (111) (200) (220) and (311) hkl planes are taken in to consideration for the calculation of residual stresses. $S_{1(hkl)}$ and $\frac{1}{2} S_{2(hkl)}$ are orientation dependent elastic constants and they are calculated using Kröner model [27] using single crystal elastic constants of aluminum. Residual

stress σ_{11} is calculated using a least square regression fitting of $a_{<hkl>}$ vs. $\sin^2\psi$ data as described in [28].

Fig. 7 shows the plot of $a_{<hkl>}$ vs. $\sin^2\psi$ data for various incidence angles. For each incidence angle, three measurements were taken. It was observed that the error bar for incidence angles 5° and 7° is higher than that of 8.5° and it was attributed to lower ratio of peak intensity to background intensity, in contrast to grazing incidence angle 8.5° (Fig. 2).

The orientation dependent diffraction elastic constants calculated using self-consistent Kröner model for different {hkl} planes of aluminum is shown in Fig. 8 as a function of orientation vector $\Gamma_{(hkl)}$. The orientation vector is defined as $\Gamma_{(hkl)} = \frac{h^2k^2+k^2l^2+l^2h^2}{(h^2+k^2+l^2)^2}$. The precise lattice parameter a_o was calculated to be 4.061 ± 0.002 Å. Least square fitting of the data was done using a fitting function described in [28] to obtain the residual stresses. The comparison between $a_{<hkl>}$ measured experimentally and calculated using the residual stress values obtained using the fitting function is shown in Fig. 7 and the values are in good agreement.

3.4. Residual stress gradient

In order to obtain residual stress gradient for the coated-substrate system, it is necessary to precisely estimate the penetration depth from which the residual stress is calculated using GIXRD. Raman spectroscopy is a surface characterization technique and signals are obtained from a few hundreds of nanometer depth from the surface [29]. However, in the case of X-ray diffraction, penetration depth is in the order of microns, and hence residual stress gradient as a function of depth is
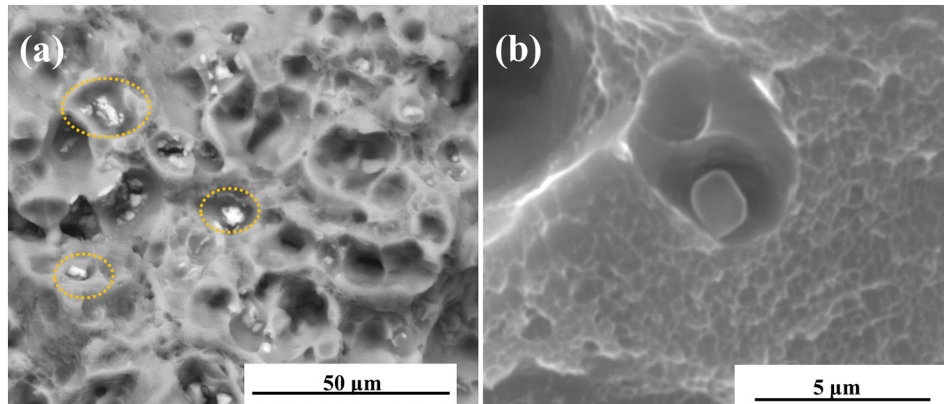

Fig. 12. Dimple nucleation sites in the final overload fracture zone of fatigue fractured samples.

(a) Uncoated, Methanol   **(b) Coated, Air**   **(c) Coated, Methanol**
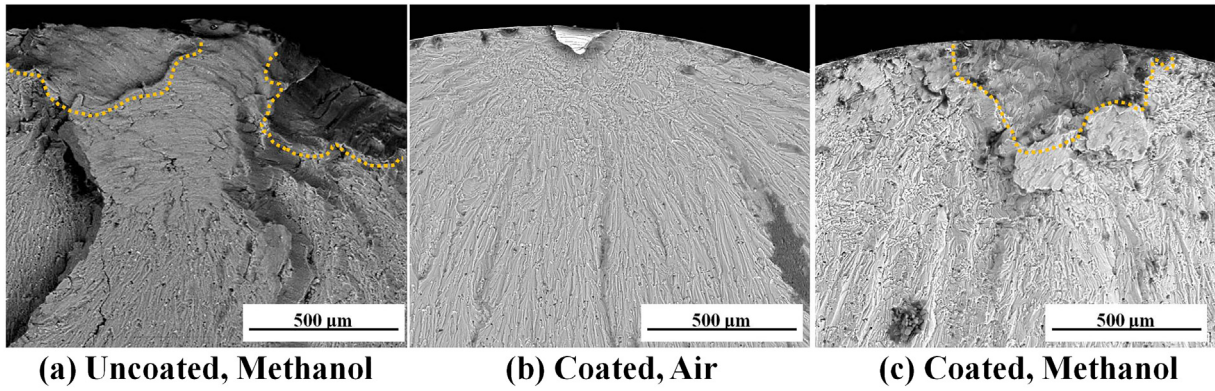
Fig. 13. Crack initiation region of fatigue tested samples in air and methanol environment.

evaluated from Bragg reflection of substrate aluminum peaks. For the precise estimation of penetration depth (t), as a function of grazing incidence angle α, the following formulation was used [28].

$$t = \left(\frac{\mu_t}{\sin\alpha} + \frac{\mu_t}{\sin(2\theta_{\{hkl\}} - \alpha)} \right)^{-1} \qquad (4)$$

where, μ_t is the total linear absorption co-efficient of the material, α is the incidence angle and $\theta_{\{hkl\}}$ is the Bragg angle of $\{hkl\}$ plane of the aluminum substrate.

Since the incoming X-ray radiation is absorbed by the coating and substrate, the total linear absorption co-efficient of the coated-substrate materials system is given by Eq. (5).

$$\mu_t = \mu_{coating} + \mu_{substrate} \qquad (5)$$

Linear absorption coefficient of the coating and the substrate is estimated from the mass absorption coefficients of the material system. The mass absorption coefficients of various elements present in the coating (based on the SEM-EDS data) and substrate are obtained from NIST standard database [30]. The densities of coating and the aluminum substrate used for the estimation of linear absorption coefficient are 2.2 g/cm^3 and 2.8 g/cm^3 respectively. The density of the coating was estimated using empirical relations from sp^3 volume fraction and I_D/I_G ratio of hydrogenated amorphous carbon (a-C: H) from the Raman spectroscopy results [31]. I_D/I_G ratio is evaluated for the DLC coating is around 0.47 $\pm$ 0.02. The volume fraction of sp^3 content is 0.51, which is inferred from the ratio of intensity of D-band and G-band (I_D/I_G) respectively [32]. The calculated total absorption coefficient is $\mu_t =$

429.2 cm^{-1} and the corresponding linear absorption coefficients of coating and the substrate for the Cu K$_\alpha$ radiation were estimated to be 282.9 cm^{-1} and 146.3 cm^{-1} respectively.

The penetration depths were calculated by substituting the values of linear absorption coefficients and angles of incidence using Eq. (4). The penetration depths for various incidence angles along with the corresponding residual stresses calculated using GIXRD data are shown in Fig. 9. Similarly, for Raman spectroscopy the maximum penetration depth achievable is around 200 nm and the corresponding residual stress calculated is included in Fig. 9. The residual stresses obtained by Raman spectroscopy and GIXRD as shown in Fig. 9, exemplify a consistent trend. A linear fit to the data with goodness of fit of 0.9 validates the use of Raman spectroscopy.

3.5. Fatigue and fractography of coated and uncoated samples

DLC coated and uncoated fatigue specimens tested in air and methanol environments at various applied stress magnitudes ranging from 200 MPa to 240 MPa are shown in Fig. 10. DLC coated specimens tested in air showed better fatigue performance, when compared to the coated specimens tested in methanol environment, thus corroborating the environmental influence on the fatigue behavior. In addition, substrate surface finish prior to coating also profoundly influenced the fatigue life of tested components. For instance, samples subjected to diamond polishing prior to coating deposition showed better fatigue behavior even at higher alternating stresses compared with 1200 grit polished samples tested in air environment.

Irrespective of testing environments and sample surface conditions, post-mortem fractographic analysis revealed characteristics fatigue features such as (i) crack initiation site at surface or sub-surface region (ii)
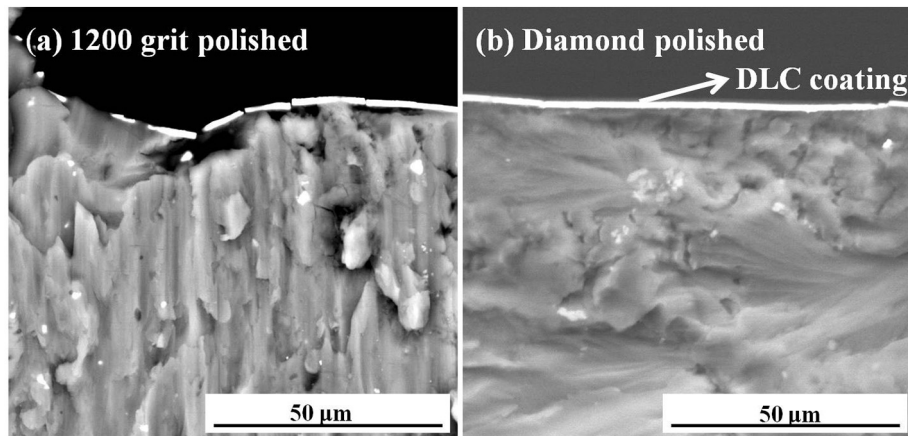

Fig. 14. Coating adherence of fatigue tested samples in air as a function of substrate surface finish condition.

crack propagation zone and (iii) final overload fracture. Each zone was clearly delineated in all the fatigue fractured specimens as shown in Fig. 11. Methanol affected regions are evident in uncoated tested samples when exposed to chemical environment, in addition to prominent crack initiation site (Fig. 11a). Micron-sized dimples were observed in the final overload fracture zone (Fig. 12a). The nucleation sites for each of the dimples were found to be iron-based constituents revealed through energy-dispersive spectroscopy. The size of these dispersoids is around 2 to 3 μm which are located inside the micro-dimples as shown in Fig. 12b. Magnified sections of the crack initiation site of all the samples are shown in Fig. 13 to understand the environmental impact on the fatigue behavior of aluminum alloys. Fractographic images of uncoated samples tested in methanol environment revealed severe damage and crater-like formation at the crack initiation site (Fig. 13a). The methanol-mediated damage area at the crack initiation zone is around 250 μm deep with cracks originating at the subsurface regions. Several secondary cracks were observed along the outer rim of the fracture surface of the failed samples. In addition, multiple crack initiation sites resulted in parallel coplanar crack-fronts, exemplifying the aggressiveness of the methanol environment.

The DLC coated samples tested in air (Fig. 13b), showed smooth fracture surface and relatively has less damage area, in contrast to uncoated samples tested in methanol. DLC coated samples in methanol environment (Fig. 13c) also revealed crater-like formation at the crack initiation site, when compared to uncoated samples tested in similar environment. However, the fracture surface is smooth and the severity of the damage is less, in contrast to the uncoated samples in methanol environment.

The coating adhesion with respect to substrate surface finish condition, prior to deposition was studied for fatigue samples tested in air environment. The rough surface obtained using 1200 grit polishing prior to DLC coating, showed extensive coating delamination and cracking at the initiation site (Fig. 14a).

In contrast, diamond polishing prior to DLC deposition guaranteed better adherence, since minimal damage is observed at the crack initiation site (Fig. 14b). Furthermore, improved adhesion and coating integrity of diamond polished samples prior to coating also resulted in superior fatigue performance than 1200 grit polished samples as shown in Fig. 10.

4. Discussion

The evaluation of residual stresses is important, since high compressive residual stresses will lead to failures such as spallation and cracking, resulting in loss of mechanical reliability of the coatings. The origin of residual stresses in coated-substrate system is broadly classified in to intrinsic and thermal stresses. The thermal stresses (σ_t) are primarily attributed to the coefficient of thermal expansion mismatch (CTE) between the coating (α_c) and the substrate (α_s) respectively.

$$\sigma_t = \frac{E_C}{1-\nu_C} \int_{RT}^{T} (\alpha_C - \alpha_S) dT \qquad (6)$$

E_c and ν_c are the elastic modulus and Poisson's ratio of the coating and T is the deposition temperature (180 °C) encountered during DLC coating deposition and RT is the room temperature. The thermal expansion coefficient of coating (α_c) largely depends upon the bonding nature and hence the CTE value was obtained from the literature based on the sp^2 concentration in the DLC layer [33]. The thermal stresses quantified from the coefficient of thermal expansion mismatch between the substrate and coating is 0.7 GPa, which is around 62% of the total residual stress of DLC coating estimated from the Raman spectroscopy. The magnitude of thermal stress is minimal due to lower deposition temperature encountered during DLC deposition.
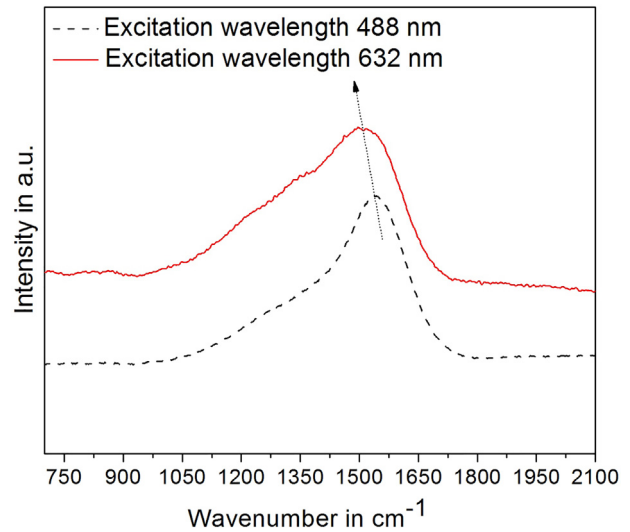

Fig. 15. Raman spectra of DLC coating as a function of excitation wavelength.

Intrinsic stresses are due to interfacial and structural mismatch between the coating and the substrate respectively [34]. Though, the evaluation of thermal stresses is straight forward from the CTE mismatch, quantification of intrinsic stresses often poses a challenge. Intrinsic stresses are growth-induced during deposition technique and its magnitude depends upon various factors such as morphology, crystallinity, structural misfit and degree of disorder in the coating. Since the coating is amorphous in nature, the structural misfit between the coating and the aluminum substrate is minimized. However, the disorder in bonding nature is invariably induced during deposition and contributes to the overall magnitude of the residual stresses. Multi-wavelength Raman analysis was utilized to quantify the degree of disorder in the DLC coating using G-peak dispersion at 488 and 632 nm respectively. It is evident from Fig. 15 that, DLC coating with a particular sp^2 configuration yielded different spectrum as a function excitation wavelength used. Due to linear relation between the G-peak wavenumber and the excitation wavelength, dispersion is calculated from the following relation (Eq. (7)). Dispersion of G-peak was around 0.13 cm^{-1}/nm, whereas zero dispersion is observed in the case of defect-free pure graphite and for tetrahedral amorphous carbon (sp^3 content > 85%) as high as 0.3 cm^{-1}/nm is reported [32]. Thus, the observed disorder in the DLC coating contributed to the total residual stresses, in addition to thermal
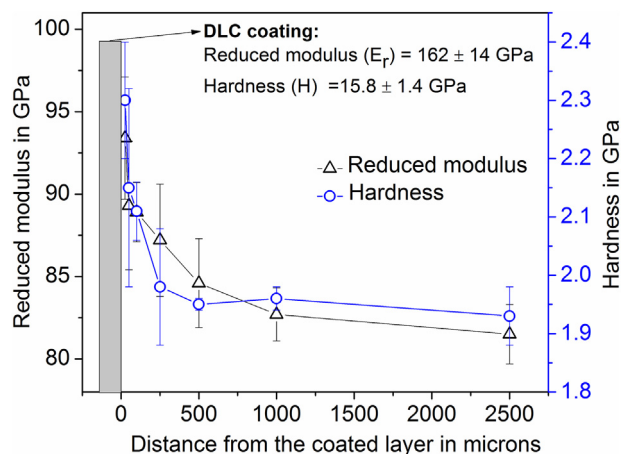

Fig. 16. Reduced modulus and nano-hardness gradient as a function of distance from the coating.

Table 4
Percentage residual stress relaxation of DLC coated samples upon fatigue loading.

Stress amplitude in MPa	Environment	Substrate surface condition	Number of cycles to failure	G peak position after fatigue deformation in cm^{-1}	Residual stress in GPa after fatigue deformation
240	Air	Diamond polished	9,131,116	1547.1 ± 0.4	−0.43
240	Methanol	1200 grit polished	3,458,359	1548.2 ± 0.4	−0.66

stresses generated due to CTE mismatch between the coating and the substrate.

$$\text{Dispersion } (\text{cm}^{-1}/\text{nm})$$
$$= \frac{\text{G peak position at 488 – G peak position at 632}}{632 - 488} \tag{7}$$

Residual stress gradient generated due to DLC coating deposition was measured experimentally using complementary Raman and GIXRD techniques. Low surface compressive residual stresses and low interfacial stresses are essential for the coating adherence, reliability and performance in complex service environments. Furthermore, in a recent published literature, CrN coating with low interfacial stresses and with a low through-thickness stress gradient showed better scratch resistance behavior over the steel substrate [35]. In the present work, tungsten-incorporated bi-layer architecture with lower average surface residual stresses of −1.12 GPa (compressive) and lower interfacial residual stress of −840 MPa (measured using GIXRD technique from the aluminum substrate peak) is proposed to improve the adhesion of DLC layer over the aluminum substrate. Through controlled optimization of bias voltage, flow rate of argon and hydrocarbon mixture, morphologically distinct bi-layer (Fig. 4) with compositional gradience was deposited with superior adhesion.

Furthermore, residual stress gradient data is of vital significance, since it can be used as an input parameter for numerical modeling of coated engineering components such as spur gears for fatigue life predictions [36]. Similar trends were observed, when the indentation hardness and reduced modulus were measured as a function of distance from the DLC coating on the cross-section of coated samples (Fig. 16). The hardness and reduced modulus monotonically decreased and asymptotically approaches that of the substrate when the indentation is performed progressively away from the DLC layer. This further substantiates the observed residual stress gradient measured using Raman and GIXRD techniques (Fig. 9).

In order to probe the residual stress relaxation upon fatigue loading, Raman spectroscopy was carried out and the stress relaxation response was recorded at 100 μm away from the fracture end in the gage section of tested samples. It is observed that diamond polished and coated sample tested in air revealed greater stress relaxation in contrast to 1200 grit polished samples tested in a methanol environment. This also substantiates the increased fatigue performance of diamond polished and coated samples tested in air as shown in Fig. 10. This indicates that, the amount of plastic deformation encountered during fatigue deformation resulted in stress relaxation, which caused the peak shift of G-band of DLC coated layer (Table 4). It is also evident from fractographic results that, no coating delamination was observed for diamond polished samples in contrast to 1200 grit samples (Fig. 14). Thus, by quantifying the magnitude of Raman shift, the damage accumulated during deformation can be probed by means of non-destructive analysis.

H^3/E^{*2}, which is a measure of resistance to plastic deformation is estimated from nano-indentation hardness and reduced modulus respectively. Higher the ratio, higher is the resistance to plastic deformation and hence less complaint to the substrate deformation during fatigue loading. The ratio obtained in the present investigation is around 0.1, which is lower than many hard coatings such as diamond, nano-crystalline TiN/Si$_3$N$_4$, Ti-B-N and Ti-B-C respectively [37]. Thus, the coating is more compliant to substrate deformation and hence good fatigue properties are expected, provided good adherence of coating is

achieved. In addition to optimized DLC deposition parameters to obtain adherent coating, surface condition of the substrate prior to coating deposition also plays a vital role in influencing the material behavior under fatigue loading conditions.

5. Summary and conclusions

In this work, the influence of testing environments, substrate surface conditions and residual stresses due to DLC coating on the fatigue behavior of aluminum alloy 7075-T6 were investigated. W-incorporated morphologically distinct diamond-like carbon (DLC) bi-layer of 2 μm in thickness with compositional gradience was coated over the aluminum substrate to improve coating adhesion. The residual stresses due to coating deposition were calculated using Raman spectroscopy and it was compressive in nature with a value of −1.13 ± 0.16 GPa. Furthermore, Raman spectroscopy is used in conjunction with multi-reflection GIXRD technique to obtain depth-resolved residual stresses of coated-substrate system up to 3 μm in depth. A linear trend-line plot of the residual stresses obtained using Raman spectroscopy and GIXRD technique revealed a good agreement between the two measurement methods. Improvement in fatigue performance was observed for DLC coated specimens in air, with smooth surface finish condition prior to DLC deposition. However, poor fatigue behavior was observed for DLC coated and fatigue tested samples in methanol environment which corroborates environmental induced fatigue crack initiation. Furthermore, Raman spectroscopy technique was utilized to probe the gage section of fatigue failed specimens in order to understand the stress relaxation in the coating upon fatigue loading. Good correlation exists between the degree of residual stress relaxation and the fatigue properties such as number of cycles to failure. Nano-indentation results of DLC coating showed better compliance to plastic deformation with H^3/E^{*2} value of 0.1 and hence better improvement in fatigue properties in contrast to other hard coatings.

Author contributions

N.S. and L.K.B. conceived the idea and designed the experiments. R.K. supervised all the experiments and analysis. S.B. optimized coating deposition parameters and carried out fatigue experiments in air and aggressive environments. N.S. and L.K.B. carried out SEM fractography, residual stress measurement using GIXRD and Raman spectroscopy in addition to nano-indentation experiment and analyzed all the results. All authors helped in the preparation of draft paper. N.S. wrote the manuscript and all authors discussed the results and commented on the manuscript.

References

[1] U. Zupanc, J. Grum, Effect of pitting corrosion on fatigue performance of shot-peened aluminium alloy 7075-T651, J. Mater. Process. Technol. 210 (2010) 1197–1202.
[2] T.P. Savas, J.C. Earthman, Fatigue crack nucleation studies on sulfuric acid anodized 7075-T73 aluminum, J. Mater. Eng. Perform. 23 (2014) 2131–2138.
[3] S. Baragetti, N. Srinivasan, L.K. Bhaskar, R. Kumar, Influence of environment, residual stresses on the fatigue behavior of 7075-T6 aluminum alloy, Key Eng. Mater. 754 (2017) 3–6.
[4] S. Baragetti, R. Gerosa, F. Villa, Physical vapour deposition of diamond like carbon coatings on a 7075-T6 substrate for corrosion protection at long and short fatigue lives, Int. J. Struct. Integr. 8 (2017) 576–584.

[5] M.A. Rahmat, R.H. Oskouei, R.N. Ibrahim, R.K.S. Raman, The effect of electroless Ni–P coatings on the fatigue life of Al 7075-T6 fastener holes with symmetrical slits, Int. J. Fatigue 52 (2013) 30–38.

[6] R.H. Oskouei, R.N. Ibrahim, M.R. Barati, An experimental study on the characteristics and delamination of TiN coatings deposited on Al 7075-T6 under fatigue cycling, Thin Solid Films 526 (2012) 155–162.

[7] E.S. Puchi-Cabrera, M.H. Staia, J. Lesage, L. Gil, C. Villalobos-Gutiérrez, J. La Barbera-Sosa, E.A. Ochoa-Pérez, E. Le Bourhis, Fatigue behavior of AA7075-T6 aluminum alloy coated with ZrN by PVD, Int. J. Fatigue 30 (2008) 1220–1230.

[8] R.H. Oskouei, R.N. Ibrahim, Restoring the tensile properties of PVD-TiN coated Al 7075-T6 using a post heat treatment, Surf. Coat. Technol. 205 (2011) 3967–3973.

[9] A. Erdemir, C. Donnet, Tribology of diamond-like carbon films: recent progress and future prospects, J. Phys. D. Appl. Phys. 39 (2006) R311–R327.

[10] H. Hetzner, C. Schmid, S. Tremmel, K. Durst, S. Wartzack, Empirical-statistical study on the relationship between deposition parameters, process variables, deposition rate and mechanical properties of a-C: H: W coatings, Coatings 4 (2014) 772–795.

[11] X. Li, L. Sun, P. Guo, P. Ke, A. Wang, Structure and residual stress evolution of Ti/Al, Cr/Al or W/Al co-doped amorphous carbon nanocomposite films: insights from ab initio calculations, Mater. Des. 89 (2016) 1123–1129.

[12] J. Schaufler, K. Durst, T. Haas, R. Nolte, H.W. Höppel, M. Göken, The influence of hydrogenated amorphous carbon coatings (a-C:H) on the fatigue life of coated steel specimens, Int. J. Fatigue 37 (2012) 1–7.

[13] C. Malerba, M. Valentini, C.L.A. Ricardo, A. Rinaldi, E. Cappelletto, P. Scardi, A. Mittiga, Blistering in Cu_2ZnSnS_4 thin films: correlation with residual stresses, Mater. Des. 108 (2016) 725–735.

[14] A.M. Korsunsky, E. Salvati, A.G.J. Lunt, T. Sui, M.Z. Mughal, R. Daniel, J. Keckes, E. Bemporad, M. Sebastiani, Nanoscale residual stress depth profiling by Focused Ion Beam milling and eigenstrain analysis, Mater. Des. 145 (2018) 55–64.

[15] M. Krottenthaler, C. Schmid, J. Schaufler, K. Durst, M. Göken, A simple method for residual stress measurements in thin films by means of focused ion beam milling and digital image correlation, Surf. Coat. Technol. 215 (2013) 247–252.

[16] J.W. Ager III, S. Anders, A. Anders, I.G. Brown, Effect of intrinsic growth stress on the Raman spectra of vacuum-arc-deposited amorphous carbon films, Appl. Phys. Lett. 66 (1995) 3444.

[17] M. Kahn, M. Cekada, R. Berghauser, W. Waldhauser, C. Bauer, C. Mitterer, E. Brandstätter, Accurate Raman spectroscopy of diamond-like carbon films deposited by an anode layer source, Diam. Relat. Mater. 17 (2008) 1647–1651.

[18] S. Baragetti, E.V. Arcieri, Corrosion fatigue behavior of Ti-6Al-4V: chemical and mechanical driving forces, Int. J. Fatigue 112 (2018) 301–307.

[19] H. Pouraliakbar, M.R. Jandaghi, G. Khalaj, Constrained groove pressing and subsequent annealing of Al-Mn-Si alloy: microstructure evolutions, crystallographic transformations, mechanical properties, electrical conductivity and corrosion resistance, Mater. Des. 124 (2017) 34–46.

[20] H. Pouraliakbar, M.R. Jandaghi, S.J.M. Baygi, G. Khalaj, Microanalysis of crystallographic characteristics and structural transformations in SPDed Al-Mn-Si alloy by dual-straining, J. Alloys Compd. 696 (2017) 1189–1198.

[21] H. Pouraliakbar, M.R. Jandaghi, A. Heidarzadeh, M.M. Jandaghi, Constrained groove pressing, cold-rolling, and post-deformation isothermal annealing: consequences of their synergy on material behavior, Mater. Chem. Phys. 206 (2018) 85–93.

[22] N. Srinivasan, R. Velmurugan, R. Kumar, S.K. Singh, B. Pant, Deformation behavior of commercially pure (CP) titanium under equi-biaxial tension, Mater. Sci. Eng. A 674 (2016) 540–551.

[23] A.-Y. Wang, H.-S. Ahn, K.-R. Lee, J.-P. Ahn, Unusual stress behavior in W-incorporated hydrogenated amorphous carbon films, Appl. Phys. Lett. 86 (2005), 111902. .

[24] J.A. Thornton, High rate thick film growth, Annu. Rev. Mater. Sci. 7 (1977) 239–260.

[25] Y.S. Zou, K. Zhou, Y.F. Wu, H. Yang, K. Cang, G.H. Song, Structure, mechanical and tribological properties of diamond-like carbon films on aluminum alloy by arc ion plating, Vacuum 86 (2012) 1141–1146.

[26] M. Marciszko, A. Baczmanski, C. Braham, M. Wrobel, S. Wronski, G. Cios, Stress measurements by multi-reflection grazing-incidence X-ray diffraction method (MGIXD) using different radiation wavelengths and different incident angles, Acta Mater. 123 (2017) 157–166.

[27] M.E. Fitzpatrick, A. Lodini, Analysis of residual stress by diffraction using neutron and synchrotron radiation, in: A. Lodini (Ed.), Calculation of Residual Stress From Measured Strain, Taylor & Francis, London and New York 2003, p. 55.

[28] A. Baczmanski, C. Braham, W. Seiler, N. Shiraki, Multi-reflection method and grazing incidence geometry used for stress measurement by X-ray diffraction, Surf. Coat. Technol. 182 (2004) 43–54.

[29] S.R. Sails, D.J. Gardiner, M. Bowden, J. Savage, Don Rodway, Monitoring the quality of diamond films using Raman spectra excited at 514.5 nm and 633 nm, Diam. Relat. Mater. 5 (1996) 589–591.

[30] NIST USA, X-ray mass attenuation coefficient, https://physics.nist.gov/PhysRefData/XrayMassCoef/tab3.html, Accessed date: 27 January 2018.

[31] A.C. Ferrari, Diamond-like carbon for magnetic storage disks, Surf. Coat. Technol. 180 (2004) 190–206.

[32] A.C. Ferrari, John Robertson, Raman spectroscopy of amorphous nanostructured, diamond-like carbon and nanodiamond, Philos. Trans. R. Soc. Lond. A 362 (2004) 2477–2512.

[33] A. Champi, R.G. Lacerda, G.A. Viana, F.C. Marques, Thermal expansion dependence on the sp^2 concentration of amorphous carbon and carbon nitride, J. Non-Cryst. Solids 338 (2004) 499–502.

[34] E. Liu, L. Li, B. Blanpain, J.P. Celis, Residual stresses of diamond and diamond-like carbon films, J. Appl. Phys. 98 (2005), 073515. .

[35] M. Renzelli, M.Z. Mughal, M. Sebastiani, E. Bemporad, Design, fabrication and characterization of multilayer Cr-CrN thin coatings with tailored residual stress profiles, Mater. Des. 112 (2016) 162–171.

[36] S. Baragetti, F. Tordini, A numerical study on the fatigue and rolling contact fatigue behaviour of PVD-coated steel and titanium spur gears, Eng. Comput. 27 (2011) 127–137.

[37] J. Musil, Hard and superhard nanocomposite coatings, Surf. Coat. Technol. 125 (2000) 322–330.